Electrical and gas sensing properties of polyaniline functionalized single-walled carbon nanotubes

2010 Nanotechnology 21 075502

(http://iopscience.iop.org/0957-4484/21/7/075502)

Nanotechnology **21** (2010) 075502 (7pp) doi:10.1088/0957-4484/21/7/075502

Electrical and gas sensing properties of polyaniline functionalized single-walled carbon nanotubes

Jae-Hong Lim[1], Nopparat Phiboolsirichit[1], Syed Mubeen[1], Marc A Deshusses[2,3], Ashok Mulchandani[1] and Nosang V Myung[1,3]

[1] Department of Chemical and Environmental Engineering and Center for Nanoscale Science and Engineering, University of California-Riverside, Riverside, CA 92521, USA
[2] Department of Civil and Environmental Engineering, Box 90287, Duke University, Durham, NC 27708, USA

E-mail: marc.deshusses@duke.edu and myung@engr.ucr.edu

Received 1 December 2009, in final form 21 December 2009
Published 18 January 2010
Online at stacks.iop.org/Nano/21/075502

Abstract
Electrical and gas sensing properties of single-walled carbon nanotube networks functionalized with polyaniline (PANI–SWNTs) were systematically investigated to understand the gas sensing mechanisms and optimize sensing performance. The temperature-dependent electrical resistance and field-effect transistor (FET) transfer characteristics indicated that the electrical properties of PANI–SWNTs are dominated by the PANI coating. The FET transfer characteristics of PANI–SWNTs exposed to different NH_3 concentrations indicated that the dominant sensing mechanism is the deprotonation of PANI by NH_3. Sensing experiments with different gas analytes revealed that PANI–SWNTs responded positively to NH_3, and negatively to NO_2 and H_2S with sensitivities of 5.8% per ppm_v of NH_3, 1.9% per ppm_v of NO_2, and 3.6% per ppm_v of H_2S. The lower detection limits were 50, 500, and 500 ppb for NH_3, NO_2, and H_2S, respectively.

1. Introduction

Chemical gas sensors have been widely used to detect and monitor various gaseous analytes in many applications including environmental pollution, industrial emission, medical diagnosis, agriculture, public security, aeronautics, and aerospace [1]. Conventional chemical gas sensors often rely on thin/thick films of various sensing materials. However, these sensors often have a low sensitivity since they require a large amount of adsorbed gaseous molecules to affect the bulk properties of the film. Typical solid-state gas sensors usually need to be heated to temperatures exceeding 200 °C for efficient operation and to provide a measurable signal [2]. To improve sensing performance, one-dimensional (1D) nanostructures, such as carbon nanotubes and metal oxide nanowires have been employed to overcome the fundamental limitations of film based sensors. The ultrahigh surface-to-volume ratio and unique size-dependent properties of nanomaterials have resulted in very promising improvements in sensing performance. Indeed, many papers have now demonstrated sensitive detection of a wide variety of gaseous targets at room temperature with various types of nanoengineered materials [3–6].

A great deal of effort was placed on using single-walled carbon nanotubes (SWNTs) for chemiresistive gas nanosensors [4], because of their excellent electrical properties. However, gas sensors based on pristine SWNTs usually display poor sensitivity with low selectivity, a direct consequence of the lack of specific interaction between SWNTs and the target gas analyte [4]. This has stimulated research on the functionalization of SWNTs with sensitizing materials such as metals, metal oxides, and conducting polymers [7–11]. For instance, when Pd and Au nanoparticles were deposited on SWNTs, superior sensing performance toward hydrogen and hydrogen sulfide was observed at room temperature, respectively [10–13].

[3] Address for correspondence: Department of Chemical and Environmental Engineering at University of California-Riverside, Bourns Hall B353, 900 University Avenue, Riverside, CA 92521, USA.

Among conducting/conjugated polymers, polyaniline (PANI) is regarded as one of the most promising conducting polymers because of its ease of synthesis, low cost, and versatile processability [14–16]. In comparison to chemiresistive sensors made with polypyrrole, chemiresistive PANI sensors exhibited a higher sensitivity to ammonia with shorter response times [16].

A detailed review of the PANI gas sensing literatures reveals that the sensitivity of PANI based sensors increases when reducing the dimension of the sensing element from bulk/thick films to two-dimensional thin films [17, 18]. For example, the sensitivity of PANI ultrathin films toward NH_3 was seven times greater than that of PANI pellets, possibly because of the higher surface-to-volume ratio and shorter diffusion length for the ultrathin film [19, 20]. In our previous work, we demonstrated the feasibility of electrochemical functionalization of randomly oriented SWNT networks with PANI and that the resulting sensors had an excellent sensitivity to NH_3 (2.44% per ppm) at room temperature [7]. Electrochemical deposition was preferred because of its simplicity and potential for cost effective production of spatially tailored hybrid nanostructures. The thickness and morphology of the hybrid nanomaterials could be precisely controlled by adjusting deposition charge and applied potential [11, 7].

In this work, the electrical and gas sensing properties of PANI functionalized SWNTs were systematically investigated to develop a better understanding of the sensing mechanism by the measurement of temperature-dependent I–V and FET transfer characteristics. To increase transfer characteristics of SWNTs, which can further enhance the sensing performance of PANI–SWNTs, SWNT networks were AC dielectrophoretically assembled prior to the electrochemical functionalization of SWNTs. The sensitivity and detection limits of PANI–SWNT networks toward NH_3, NO_2, and H_2S were established.

2. Experiments

Suspended SWNTs in N,N-dimethylformamide (DMF) solution were prepared by first ultrasonically dispersing 10 μg ml^{-1} of carboxylated SWNTs (SWNTs–COOH 80–90% purity from Carbon Solution, Inc. (Riverside, CA)), followed by centrifugation at 31 000 G for 90 min to remove the non-soluble fraction and aggregates [7].

Microfabricated gold electrodes were fabricated on highly doped p-type silicon substrate. First, a 300 nm SiO_2 thick film was deposited on the substrate by low pressure chemical vapour deposition (LPCVD). Secondly, Cr/Au (20/180 nm) electrodes were formed using standard lift-off techniques where the width (W) and gap (L_{SD}) of the electrodes were fixed at 200 and 3 μm, respectively.

For aligned SWNTs, 0.2 μl of SWNTs suspended solution was placed on top of gold electrodes while applying 0.36 V_{RMS} at 4 MHz frequency. The resistance of the SWNT networks was adjusted by varying the deposition time. As expected, the resistance of the networks increased with decreasing the deposition time. After assembly, the devices were rinsed with deionized water and dried by gently blowing with nitrogen gas. To reduce the contact resistance between the electrodes and SWNTs, and to remove possible DMF residues, the sensors were annealed at 300 °C for 1 h in a reducing environment (i.e. 5% H_2 in N_2).

Electrochemical functionalization of SWNTs with PANI was conducted at ambient temperature with a three-electrode configuration where the SWNTs network with gold electrodes, a stainless steel tip, and chlorinated silver wire (Ag/AgCl wire) were employed as working, counter, and reference electrodes, respectively. For the electrochemical functionalization, 2 μl of deoxygenated electrolyte (i.e. aqueous solution of 0.1 M aniline and 1 M HCl) was placed on top of the SWNT networks, followed by potentiostatic electrodeposition at +1 V versus Ag/AgCl wire. The deposition charge was fixed at 0.12 mC. After the functionalization, the sensors were rinsed several times with deionized water followed by drying in a vacuum chamber.

The morphology and size distribution of SWNTs before and after the functionalization were examined using an atomic force microscope (AFM) (Veeco Innova, Santa Barbara, CA). The current–voltage (I–V) for devices was measured using a Keithley 236 measurement unit (Cleveland, OH). Thermal activation energies (E_A) were calculated from electrical resistance Arrhenius plots between 190 and 300 K after measuring temperature-dependent I–V from 30 to 300 K using a cold-finger cryogenic system (Janis CCS-350SH, Wilmington, MA). For FET transfer characteristics, the highly doped Si substrate was used as the back gate. FET measurements were performed using a Keithley 2636 measurement unit in ambient conditions. To further improve the electrical transfer characteristics of SWNT networks and investigate their effects on electrical and sensing performance of PANI–SWNTs, selective electrical breakdown of metallic SWNTs (m-SWNTs) was performed by applying high source–drain potential (V_{DS}) while minimizing the current flow in semiconducting SWNTs (s-SWNTs) by applying a positive gate voltage of 20 V.

The experimental protocol to determine the NH_3 sensing mechanism of PANI–SWNTs used a ChemFET configuration. Experiments were initiated by exposing sensors to dry air to reach the steady-state (equilibrium) baseline, followed by exposure to a fixed concentration of the analyte for 15 min and then measurement of the transfer characteristics of the sensors. Once the measurements were completed, a higher NH_3 concentration was introduced and the process was repeated. For chemiresistive sensing, a circuit composed of a load resistor and the sensor was subjected to a fixed DC voltage of 1 V. The potential across the load resistor was continuously monitored and used to calculate the resistance of the sensor by applying Ohm's law. Fieldpoint modules (National Instruments, Austin, TX) and a custom LabVIEW program were used to monitor 16 sensors continuously.

3. Results and discussion

Figures 1(a) and (b) show the AFM images for AC dielectrophoretically aligned SWNT networks before and after electrochemical functionalization with PANI, respectively.

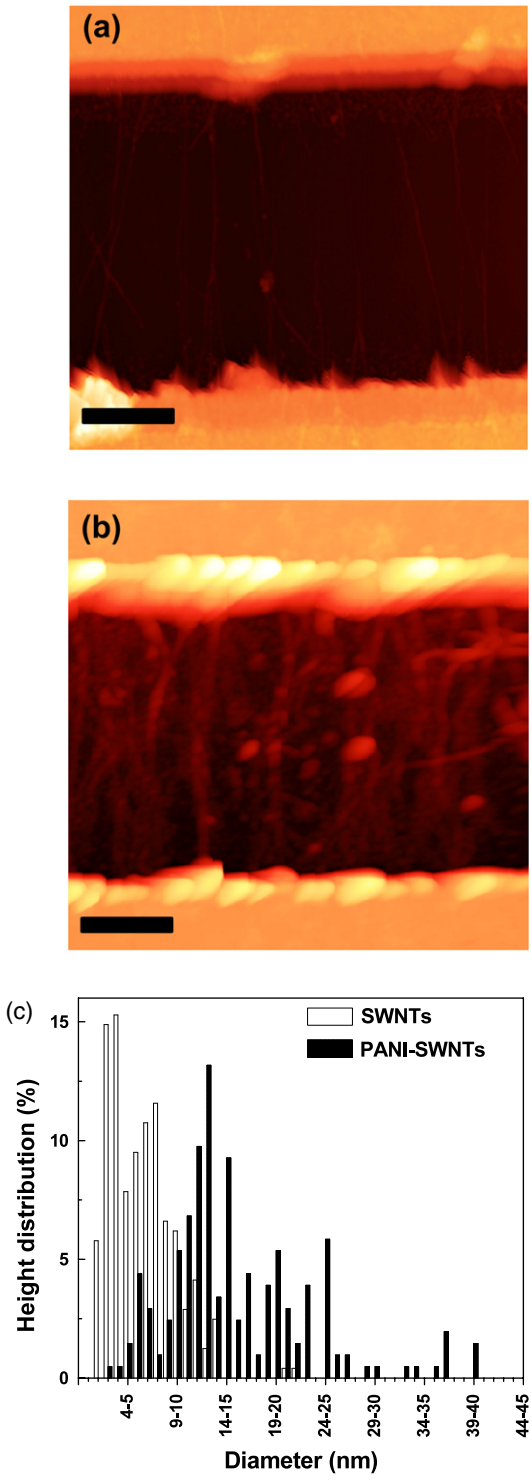

Figure 1. AFM images of (a) SWNT and (b) PANI–SWNT networks. The scale bar corresponds to 1 μm. (c) Height distribution histograms of AC aligned SWNT and PANI–SWNT networks without the breakdown process. The deposition charge of PANI on SWNT networks was fixed at 0.12 mC.

(This figure is in colour only in the electronic version)

Compared to the drop-cast SWNTs which are randomly oriented SWNT networks, AC dielectrophoresis resulted in uniform alignment of SWNTs across the electrode gap.

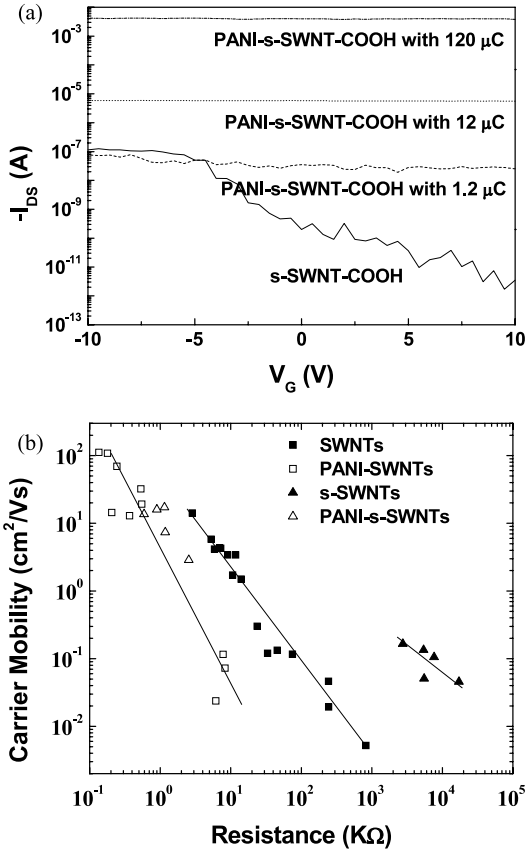

Figure 2. (a) Comparison of FET transfer characteristics of SWNT and PANI–SWNT networks with different deposition charges after the breakdown process. (b) Field-effect mobility of SWNT and PANI–SWNT networks with and without selective breakdown of m-SWNTs.

Electrodeposition of PANI is believed to nucleate at defect sites on the surface of SWNTs, followed by the growth of the formed nuclei over the SWNTs eventually forming a complete coating on the SWNTs upon continued electrodeposition. The electrodeposited PANI on SWNTs had a nodular structure where many researchers have found a correlation between polymer film surface morphology and polymer conductivity. In particular, a nodular structure has been associated with highly doped conducting films in which the nodules represent dopant-rich and highly conductive areas [21]. Figure 1(c) compares the height distribution of SWNT and PANI–SWNT networks. The mean average height increased from 6.0 nm for unfunctionalized SWNTs bundles to approximately 15.5 nm for the PANI–SWNT networks.

To further improve the FET transfer characteristics of SWNT networks and investigate their effects on the electrical properties of PANI–SWNTs, selective breakdown of m-SWNTs was conducted to leave only s-SWNTs. The transfer characteristics of s-SWNT and PANI-s-SWNT networks were compared for different amounts of PANI deposited. The results (figure 2(a)) indicate that s-SWNT networks have a clear off-state and a strong dependency on the gate bias whereas the PANI–SWNT networks showed no modulation of I_{DS} by the gate voltage, even at the lowest (1.2 μC) deposited charge.

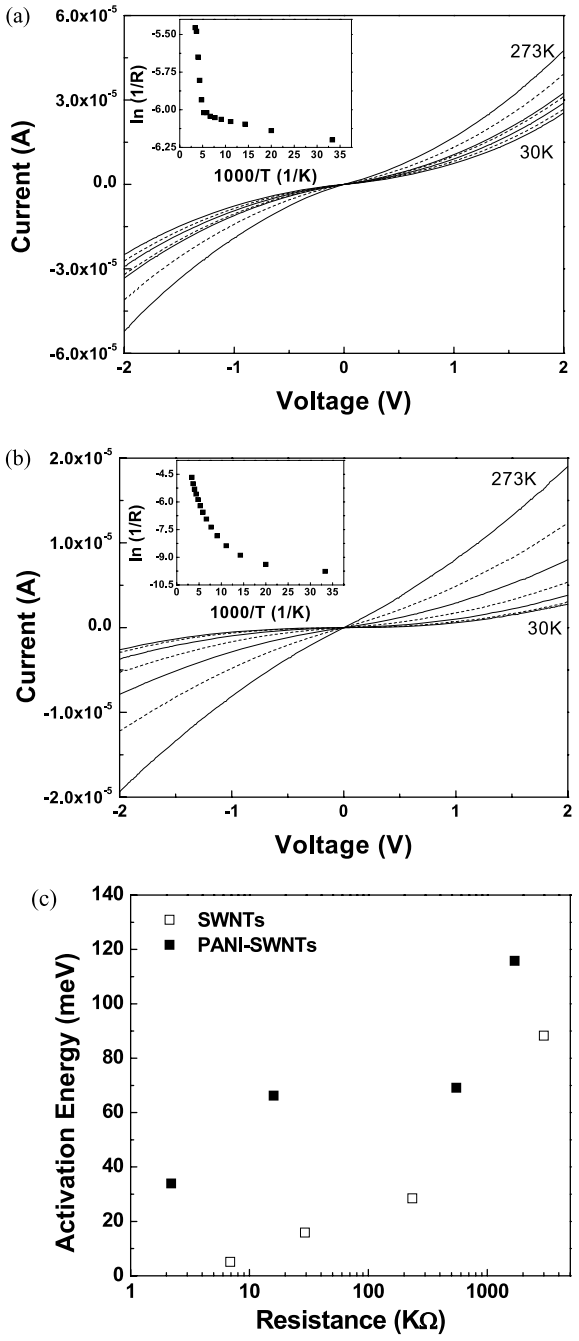

Figure 3. Temperature-dependent I–V curves for SWNT networks before (a) and after (b) PANI functionalization. The selective I–V curves at 30, 70, 110, 150, 190, 230, and 273 K are shown. The insets report the resistance change as a function of temperature. (c) Comparison of the thermal activation energy (E_A) of SWNT networks before and after PANI functionalization at the different resistances.

This is despite the fact that at 1.2 μC charge deposited, PANI did not form a continuous coating on the SWNTs as indicated by AFM (results not shown) and by the quasi-identical value of I_{DS} at low gate voltages (figure 2(a)). As expected, the current through the PANI–SWNT networks increased at the two highest deposited charges, because the PANI coating formed was continuous, resulting in an additional conducting pathway

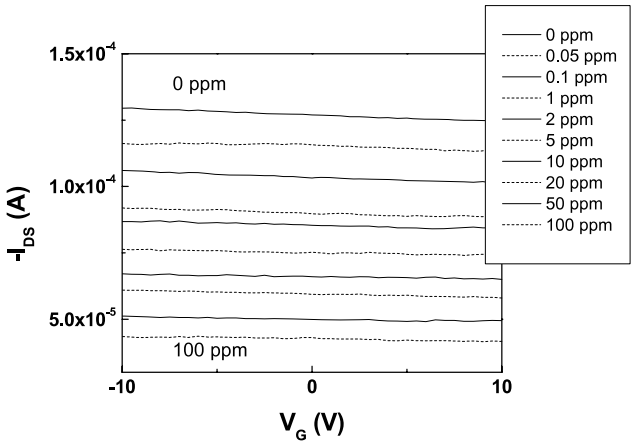

Figure 4. FET transfer characteristics of PANI–SWNT networks without the breakdown process upon exposure to different NH_3 concentration.

between electrodes. The resulting continuous PANI coating had a much higher conductivity than the unfunctionalized s-SWNT networks [22], which indicates that the majority of the current flows through the PANI instead of SWNTs after functionalization.

The field-effect mobility of the holes was calculated in the linear regime using

$$\mu = L_{SD}^2 \mathrm{d}I/\mathrm{d}V/C_G V_D \quad (1)$$

with L_{SD}, C_G, and V_D being the gap of the electrodes, the approximate capacitance, and the drain voltage, respectively [23]. Figure 2(b) shows the dependency of the field-effect mobility on the resistance of SWNTs for multiple devices. The field-effect mobility increased after the breakdown of m-SWNTs because m-SWNTs are a source of scattering centers. The field-effect mobility of PANI–SWNT networks is significantly lower than for SWNT networks at fixed resistance. In addition, the breakdown of m-SWNTs followed by PANI functionalization did not affect the electrical properties of the PANI–SWNTs networks as the same trend of field-effect mobility versus resistance was observed for PANI–SWNTs without m-SWNT breakdown (figure 2(b)). This is most probably because the current flows mainly through the continuous PANI coating.

Figure 3 shows selected temperature-dependent I–V curves for SWNT and PANI–SWNT networks. At room temperature, SWNT networks have a non-linear I–V characteristic (figure 3(a)) which might be attributed to the Schottky barrier between SWNTs and gold electrodes [24]. On the other hand, PANI–SWNT networks have almost linear I–V characteristics at room temperature (figure 3(b)), even though there is the difference in energy between the work function of Au metal (5.1 eV) and the highest occupied molecular orbital (HOMO) (around 5.5 eV) of PANI [25]. This may be attributed to the high conductivity of PANI, which might make tunneling the dominant transport mechanism [26]. As temperature decreases, non-linearity increases, possibly because of a decrease of tunneling probability due to the

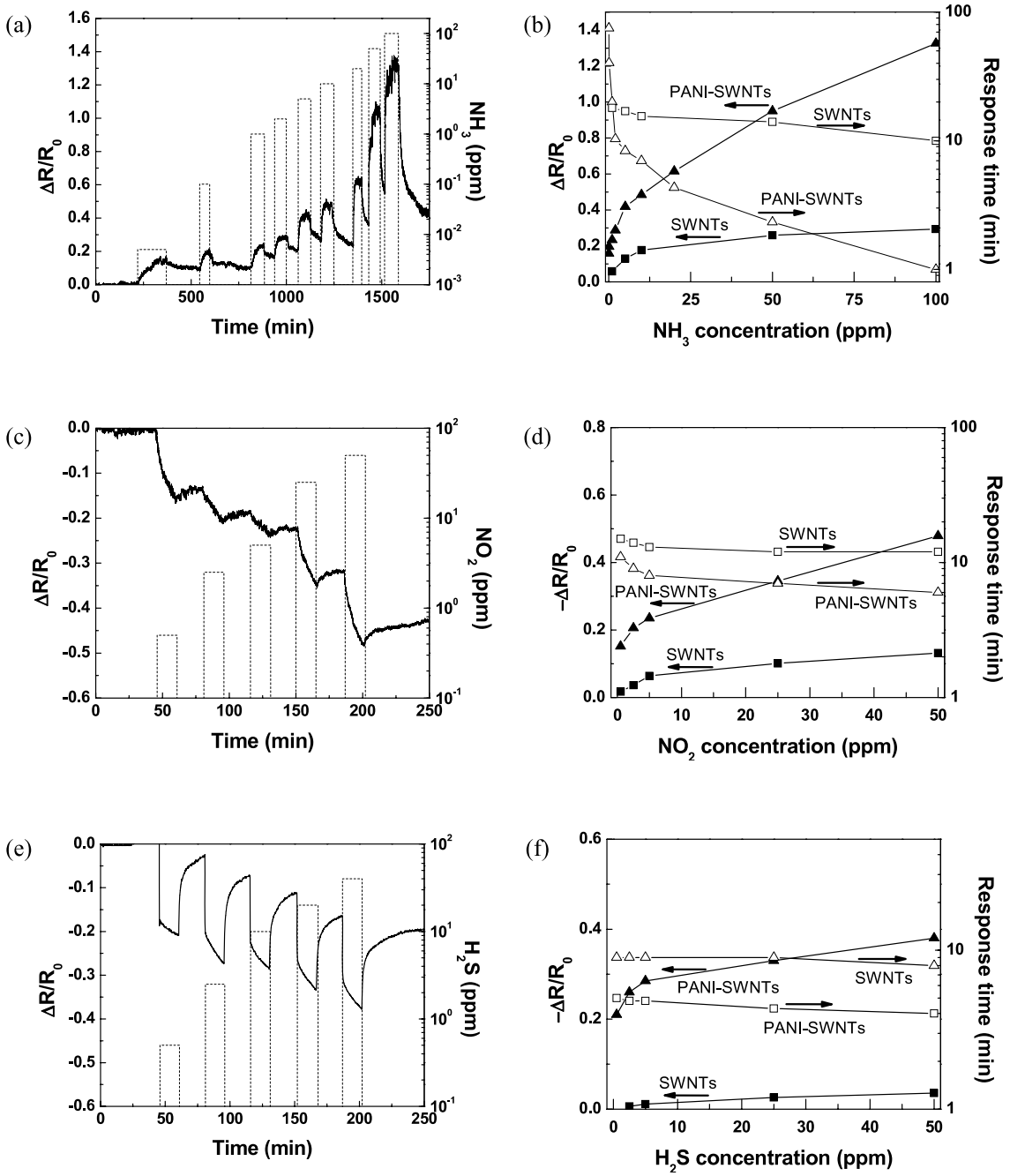

Figure 5. Electrical resistance change (solid line) as a function of time and inlet analyte gas concentration (dashed line), and comparison of sensor response as $\Delta R/R_0$ (closed symbols) and response time (open symbol) between SWNT (■□) and PANI–SWNT (▲△) based sensors without the breakdown process upon the exposure of different NH_3 ((a) and (b), respectively), NO_2 ((c) and (d), respectively), and H_2S ((e) and (f), respectively) concentrations.

decrease of carrier concentration [27]. Figure 3(c) shows the comparison of the thermal activation energy (E_A) of different SWNT and PANI–SWNT networks. Skakalova *et al* reported that the thermal E_A values at high temperature (70–300 K) of individual m- and s-SWNTs were approximately 5 meV and 29 meV, respectively [28]. Based on their work, it can be inferred that as the resistance of SWNT networks increases, the networks contain a greater portion of semiconducting SWNTs which lead to high thermal E_A [29]. The E_A of PANI–SWNT networks increased after the deposition of PANI and correlated with increases in resistance of PANI–SWNT networks. Others reported that the E_A of PANI pellets was in the range of 160–280 meV and, consistent with our findings, reported that an increase in conductivity was also associated with a decrease in thermal E_A [30].

To investigate the sensing mechanism of NH_3 by PANI–SWNT networks, a ChemFET configuration was utilized where the highly doped Si substrate was used as the back gate. Typical FET transfer characteristics of aligned PANI–SWNT networks are shown in figure 4 after exposure to different concentrations of NH_3 in air. The results show that I_{DS} (source–drain current) is not modulated by V_G (gate

voltage) and that I_{DS} drops significantly with increasing NH_3 concentration, consistent with earlier results acquired in the chemiresistive mode [9]. Unlike s-SWNT networks, I_{DS} of PANI–SWNT networks was slightly decreased by increasing V_G without a clear on–off state [29].

In the case of unfunctionalized SWNT network based NH_3 sensor, the sensing mechanism for NH_3 was attributed to a charge transfer between the electron-donating molecules and the SWNTs, which decreases the conductivity of the SWNT networks [4]. In addition, the field-effect mobility of SWNTs was reduced by 40.3% for exposure to 100 ppm NH_3. Large changes of the mobility in SWNT networks were attributed to the modulation of local work function at the metal contact and SWNTs because of a large built-in potential at the contact [31]. In the case of a PANI–SWNT network based sensor, gaseous NH_3 molecules are absorbed on PANI–SWNT networks which deprotonated N^+–H sites of polyaniline (emeraldine salt) to form NH_4^+ [32]. Deprotonation of PANI–SWNT networks causes significant conductance changes with little change of field-effect mobility. From this result, it can be concluded that the dominant sensing mechanism of PANI–SWNT networks is due to deprotonation of PANI [33].

Figure 5 reports the real-time response of AC dielectrophoretically assembled PANI–SWNT sensors to different concentrations of NH_3, NO_2, and H_2S, respectively, at room temperature (figures 5(a), (c), and (e)). Sensor calibration plots and response times are also reported (figures 5(b), (d), and (f)). The electrical resistance of the devices drastically increased upon exposure to NH_3 and then gradually decreased when exposed back to dry air (figure 5(a)). The sensor response time (defined as the time to reach 90% of the total resistance change) decreased with increasing concentration of NH_3 from 75 min at 50 ppb to 1 min at 100 ppm, while recovery time ranged from several minutes to a few hours depending on the concentration (figure 5(b)). AC aligned PANI–SWNTs show a lower detection limit of 50 ppb_v toward NH_3, where the detection limit is defined as the concentration providing a signal-to-noise ratio of at least 3. In addition, the PANI–SWNT based sensors exhibited a linear response from 50 ppb_v to 2 ppm_v with a sensitivity of 5.8% per ppm_v NH_3, which is much greater than the randomly oriented PANI–SWNT networks (2.4% per ppm_v of NH_3) [7, 34]. The greater sensitivity might be attributed to reduced nanotube to nanotube interactions and reduced accumulation of gases in the interstitial sites of the nanotubes. Figure 5(c) shows a typical real-time sensing response of PANI–SWNTs toward NO_2 where the resistance of the sensor decreased after exposure to NO_2. This is consistent with the transfer of π-electrons from PANI to the adsorbed NO_2 resulting in a positive charge for PANI and an increase in charge carriers that increases the conductivity of PANI. A typical real-time response of PANI–SWNT networks toward H_2S is shown in figures 5(e) with their sensing performance (figure 5(f)). Similar to NO_2, the resistance of the sensors decreased in the presence of the analyte. H_2S is believed to partly dissociate into H^+ and HS^- as it is a weak acid, resulting in the partial protonation of PANI, hence a decrease in the sensor's resistance. The lower detection limit of both NO_2 and H_2S was about 500 ppb which is the lowest reported for polymer based nanosensor without the incorporation of metals or metal oxides at room temperature. It is also about an order of magnitude lower than the best PANI thin film sensors [14]. Since these results indicate that the sensors exhibit significant analyte cross-sensitivity, efforts should be directed toward improving sensor selectivity e.g. by co-functionalization with other nanoengineered materials including metals and metal oxides.

4. Conclusion

Gas nanosensors fabricated by AC dielectrophoretically assembled SWNT networks, followed by electrochemical functionalization of PANI exhibited excellent gas sensing performance toward NH_3, NO_2, and H_2S at room temperature. PANI–SWNT networks displayed an increase of thermal E_A and decrease of FET mobility compared to unfunctionalized SWNT networks due to the continuous coating with PANI on SWNT networks. The dominant gas sensing mechanism of the PANI–SWNT networks is protonation/deprotonation of PANI by analytes, resulting in resistance increases or decreases. Compared to randomly oriented PANI–SWNTs, AC aligned PANI–SWNTs show greater sensitivity toward NH_3 (5.8% versus 2.4% per ppm_v of NH_3), which is attributed to better semiconducting properties. In addition, PANI–SWNT based nanosensors were shown to have superior sensitivities toward NO_2 (1.9% per ppm NO_2) and H_2S (3.6% per ppm H_2S) with low detection limits of 500 ppb_v for both NO_2 and H_2S.

Acknowledgments

We greatly acknowledge the support for this research by NIH-NIEHS (Gene-Environment Initiative through award U01 ES 016026) and DOD/DMEA through Center for Nanoscience Innovation for Defense (grant No. DOD/DMEA-H94003-06-2-0608). J-HL acknowledges overseas postdoctoral fellowship support from the Korea Research Foundation Grant (KRF-2008-357-D00165).

References

[1] Hunter G W, Chen L-Y, Neudeck P G, Knight D, Liu C-C, Wu Q-H and Zhou H-J 1997 *NASA Tech. Memo.* **107444** 1
[2] Kolmakov A, Zhang Y, Cheng G and Moskovits M 2003 *Adv. Mater.* **15** 997
[3] Kolmakov A and Moskovits M 2004 *Annu. Rev. Mater. Res.* **34** 151
[4] Kong J, Franklin N R, Zhou C, Chapline M G, Peng S, Cho K and Dai H 2000 *Science* **287** 622
[5] Zhang T, Mubeen S, Myung N V and Deshusses M A 2008 *Nanotechnology* **19** 332001
[6] Zhang T, Mubeen S, Yoo B, Myung N V and Deshusses M A 2009 *Nanotechnology* **20** 255501
[7] Zhang T, Nix M B, Yoo B-Y, Deshusses M A and Myung N V 2006 *Electroanalysis* **18** 1153
[8] Qi P, Vermesh O, Grecu M, Javey A, Wang Q, Dai H, Peng S and Cho K J 2003 *Nano Lett.* **3** 347
[9] Dong X, Fu D, Ahmed M O, Shi Y, Mhaisalkar S G, Zhang S, Moochhala S, Ho X, Rogers J A and Li L-J 2007 *Chem. Mater.* **19** 6059
[10] Kong J, Chapline M G and Dai H 2001 *Adv. Mater.* **13** 1384

[11] Mubeen S, Zhang T, Yoo B, Deshusses M A and Myung N V 2007 *J. Phys. Chem.* C **111** 6321
[12] Mubeen S, Zhang T, Chartupryaoon N, Rheem Y, Mulchandani A, Myung N V and Deshusses M A 2010 *Anal. Chem.* **82** 250
[13] Sun Y and Wang H H 2007 *Appl. Phys. Lett.* **90** 213107
[14] Agbor N E, Petty M C and Monkman A P 1995 *Sensors Actuators* B **28** 173
[15] Shirsat M D, Bangar M A, Deshusses M A, Myung N V and Mulchandani A 2009 *Appl. Phys. Lett.* **94** 083502
[16] Nicolas-Debarnot D and Poncin-Epaillard F 2003 *Anal. Chim. Acta* **475** 1
[17] Li N, Li X, Geng W, Zhang T, Zuo Y and Qiu S 2004 *J. Appl. Polym. Sci.* **93** 1597
[18] Aguilar A D, Forzani E S, Li X, Tao N, Nagahara L A, Amlani I and Tsui R 2005 *Appl. Phys. Lett.* **87** 193108
[19] Chabukswar V V, Pethkar S and Athawale A A 2001 *Sensors Actuators* B **77** 657
[20] Li D, Jiang Y, Wu Z, Chen X and Li Y 2000 *Sensors Actuators* B **66** 125
[21] Barisci J N, Stella R, Spinks G M and Wallace G G 2000 *Electrochim. Acta* **46** 519
[22] Alan G M 2001 *Angew. Chem. Int. Edn* **40** 2581
[23] Martel R, Schmidt T, Shea H R, Hertel T and Avouris P 1998 *Appl. Phys. Lett.* **73** 2447
[24] Cui X, Freitag M, Martel R, Brus L and Avouris P 2003 *Nano Lett.* **3** 783
[25] Tang S-J, Lin S-M, Chiu K-C, Wu Y-Y and Yeh J-M 2008 *J. Phys. D: Appl. Phys.* **12** 125401
[26] Bianchi R F, Cunha H N d, Faria R M, Ferreira G F L and Neto J M G 2005 *J. Phys. D: Appl. Phys.* **9** 1437
[27] Yu A Y C 1970 *Solid State Electron.* **13** 239
[28] Skakalova V, Kaiser A B, Woo Y S and Roth S 2006 *Phys. Rev.* B **74** 085403
[29] Lim J-H, Phiboolsirichit N, Mubeen S, Rheem Y, Deshusses M A, Mulchandani A and Myung N V 2009 submitted
[30] Singh R, Arora V, Tandon R P, Chandra S and Mansingh A 1998 *J. Mater. Sci.* **33** 2067
[31] Javey A, Guo J, Wang Q, Lundstrom M and Dai H 2003 *Nature* **424** 654
[32] Li X, Ju M and Li X 2004 *Sensors Actuators* B **97** 144
[33] Heller I, Janssens A M, Mannik J, Minot E D, Lemay S G and Dekker C 2008 *Nano Lett.* **8** 591
[34] Kim U J, Kim K H, Kim K T, Min Y-S and Park W 2008 *Nanotechnology* **19** 285705